The Origin and Quality of the Groundwater of the Rawadanau Basin in Serang Banten, Indonesia

**Priyo Hartanto[1]; Boy Yoseph C.S.S. Syah Alam[2];
Rachmat Fajar Lubis[3]; Hendarmawan Hendarmawan[4]**

[1] *Faculty of Geological Engineering, Universitas Padjadjaran, Jatinangor, Sumedang 45363, Indonesia; Research Center for Geotechnology, Indonesian Institute of Sciences, Jln. Sangkuriang, Bandung 40135, Indonesia, https://orcid.org/0000-0001-7759-6947*

[2] *Faculty of Geological Engineering, Universitas Padjadjaran, Jatinangor, Sumedang 45363, Indonesia*

[3] *Research Center for Geotechnology, Indonesian Institute of Sciences, Jln. Sangkuriang, Bandung 40135, Indonesia, https://orcid.org/0000-0002-5430-7169*

[4] *Faculty of Geological Engineering, Universitas Padjadjaran, Jatinangor, Sumedang 45363*

Abstract

Rawadanau is a tropical mountain swamp located in Serang, Banten, Indonesia. Rawadanau groundwater is the main source of supply for the Cilegon Banten industrial area. Knowing the origin and quality of the groundwater can help preserve existing resources. This paper aims to clarify the origin of Rawadanau groundwater with new evidence of stable isotopes (^{18}O and ^2H) and hydrochemical data. Field measurements included pH, temperature, EC, HCO_3^-, while the analyses of cations, anions and stable isotopes were carried out in the laboratory. The existing water supplies include springs, excavated wells, and river water. Cluster hierarchy analysis based on water chemistry and stable isotopes can be grouped into two clusters, cluster K (K1 and K2) and cluster L. Data $\delta^{18}O$ and δ^2H springs in Rawadanau indicate that they are of meteoric origin and that there has been evaporation from several springs. Water comes from meteoric water with a stable isotope content of $\delta^{18}O$ between -6.39 to -4.82 ‰ and δ^2H between -41.35 to -31.30 ‰, which are controlled by two main mechanisms, namely rock dissolution and evaporation dominance. Aquifers are composed of volcanic rocks with a dominant composition of porphyritic andesite, basaltic andesite, and andesite. According to the multivariate statistical analyses results other than pH and SO_4^{2-}, all parameters (cations and anions) showed a significant correlation. There are four hydrochemical facies of groundwater, namely $Ca-HCO_3$, $Ca-Mg-HCO_3$, $Mg-Ca-HCO_3$, and Na-Cl.

Keywords:

Rawadanau, groundwater, origin, stable isotope, hydrochemical facies, spring

1. Introduction

Rawadanau is a typical tropical mountain swamp surrounded by volcanoes and located 91 metres above sea level (asl). It becomes a marsh during the dry season and a lake in the rainy season. This investigation of Rawadanau groundwater is to understand its hydrochemical origin and isotope characteristics and thus help explain actual groundwater supply conditions in the study area. Groundwater is the most important freshwater resource at Rawadanau and at present, provides almost all of the water needs in the industrial area Cilegon. Rawadanau Sub-basin has an area of 375 km² (**KEMEN-ESDM, 2017**), which is the primary source of water fulfilment for the Cilegon industrial area. Groundwater reverse surface water is available almost everywhere in the area, and is used for drinking, irrigation, industries, and municipalities (**Hussain and Abed, 2019**).

As groundwater moves through rock, its chemical composition normally changes. In general, the longer groundwater remains in contact with aquifer rocks, the greater the amount of material it will take into the solution *(***Chebotarev, 1955***)*. Rawadanau also has geothermal potential, with several identified hot spring locations. More than 100 companies in the industrial area of Cilegon depend on the Rawadanau water reserves, which are collected by damming the Cidanau River (**Hartanto et al., 2019**). Existing water comes from rainwater, river water, springs flowing through several river branches before entering the Cidanau River.

The groundwater, including surface water and hot and cold springs, all indirectly come from precipitation. This proves that the groundwater is meteoric water, although some gradually infiltrates the ground and interacts with the rocks in its path. This injected water continues its journey to the saturation zone to become part of the aquifer. It is interesting to study Rawadanau Basin's hydrogeological condition because it is composed of quaternary vol-

Corresponding author: Priyo Hartanto

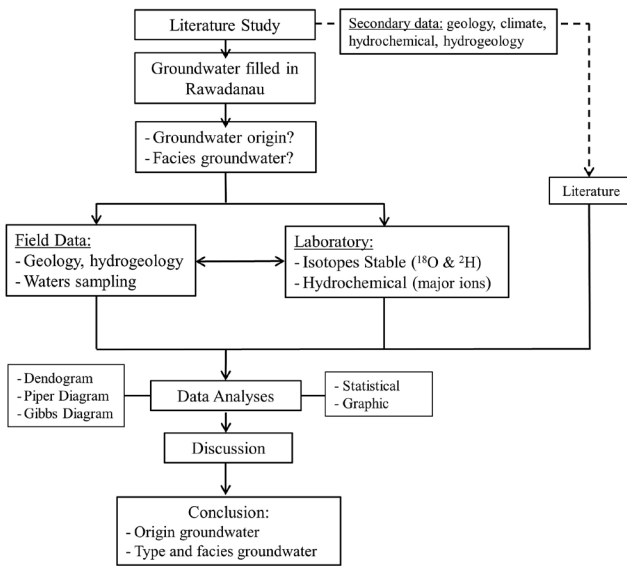*tantosuripto@gmail.com ; priyo.hartanto@lipi.go.id*

Figure 1: Workflow methodology of this research

canic products. Its lithology contributes to an aquifer layer, which is relatively influential in terms of quality. This quality is influenced by environmental and anthropogenic factors such as the geological context, climate, precipitation, the interaction between groundwater and aquifers, and human activities (**Houria et al., 2020**).

Stable isotopes can be used as tracers in the groundwater environment to understand water origin in a hydrological cycle (**Taniguchi et al., 2000**). Stable isotopes do not decay over geological time. The stable isotopes of oxygen and hydrogen in water are ^{16}O, ^{17}O, ^{18}O,

and ^{1}H and ^{2}H, respectively, whose values are expressed in δ (**Tweed et al., 2019**). Isotopes provide vital records that occur in thermal and nonthermal groundwater so they can play an essential role in hydrogeological investigations (**Oyuntsetseg et al., 2015**). Hydrochemical data and isotopes can be an effective tools to solve various hydrology and hydrogeology problems (**Chen et al., 2011; Clark and Fritz, 2013; Liu et al., 2015**). The origin, evolution, and formation of hot springs can be explained using hydrochemical and trace stable isotopes. Hydrochemistry was analyzed to determine the quality, type, dominant hydrogeochemical processes, stable isotopes of oxygen (^{18}O), and hydrogen (^{2}H) and thus clarify the origin of the groundwater.

This study aims to determine the groundwater origin of Rawadanau basin using new evidence covering the main elements of water chemistry and stable tracer isotopes (^{2}H and ^{18}O) from springs, dug wells, and surface water. The data was processed using statistics for grouping and classification of sources, using some frequently used models.

2. Methods

The research was carried out based on the results of field observations and laboratory data in the tropics. The stable isotope approach is used to understand the origin of groundwater. Meanwhile, to determine water quality, the chemical analyses of water were carried out, analysed, and modelled using SPSS statistical software. **Figure 1** shows a workflow methodology of this research.
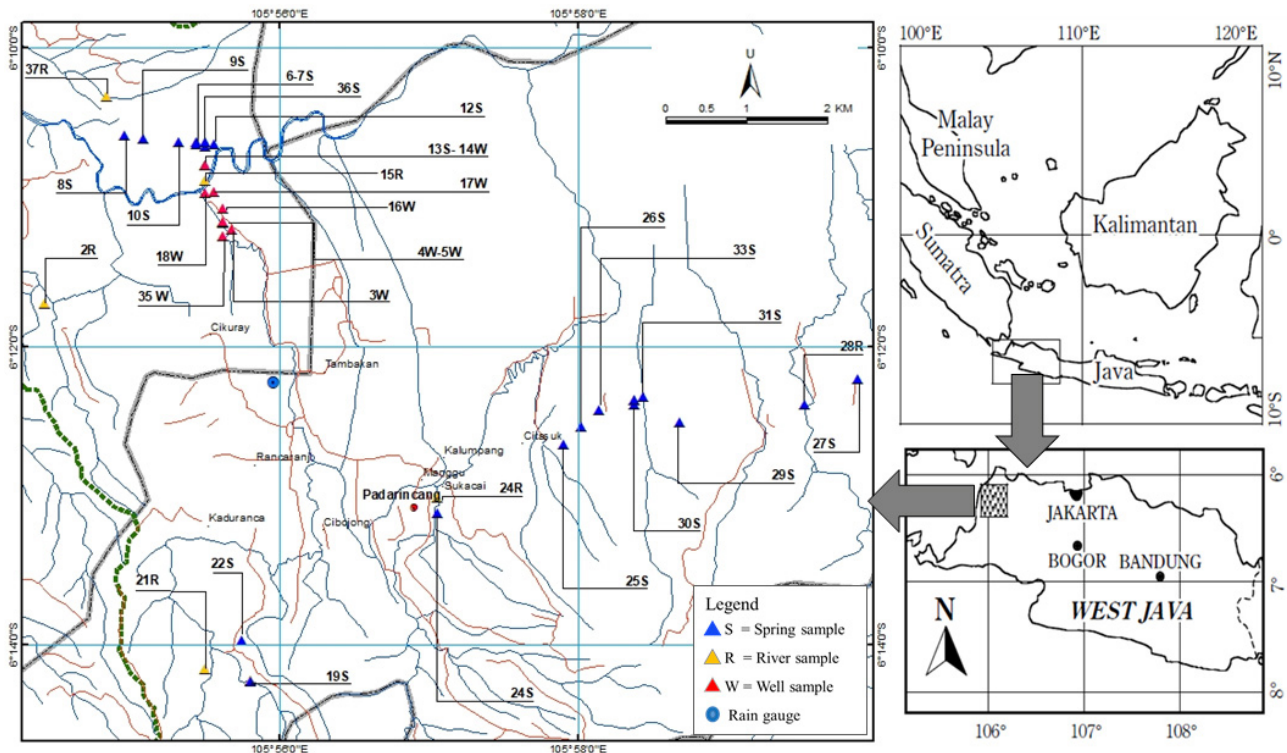
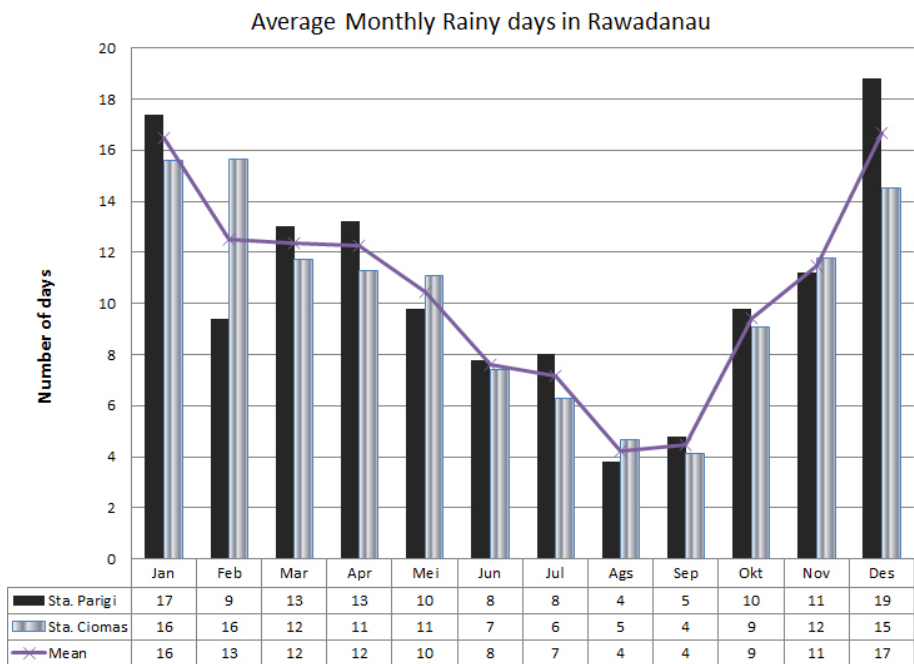

Figure 2: Locality map of the study area and sampling points.

Average Monthly Rainy days in Rawadanau

	Jan	Feb	Mar	Apr	Mei	Jun	Jul	Ags	Sep	Okt	Nov	Des
Sta. Parigi	17	9	13	13	10	8	8	4	5	10	11	19
Sta. Ciomas	16	16	12	11	11	7	6	5	4	9	12	15
Mean	16	13	12	12	10	8	7	4	4	9	11	17

Figure 3: Average monthly rainy days in Rawadanau.

Avarage Monthly Rainfall in Rawadanau (mm/month)

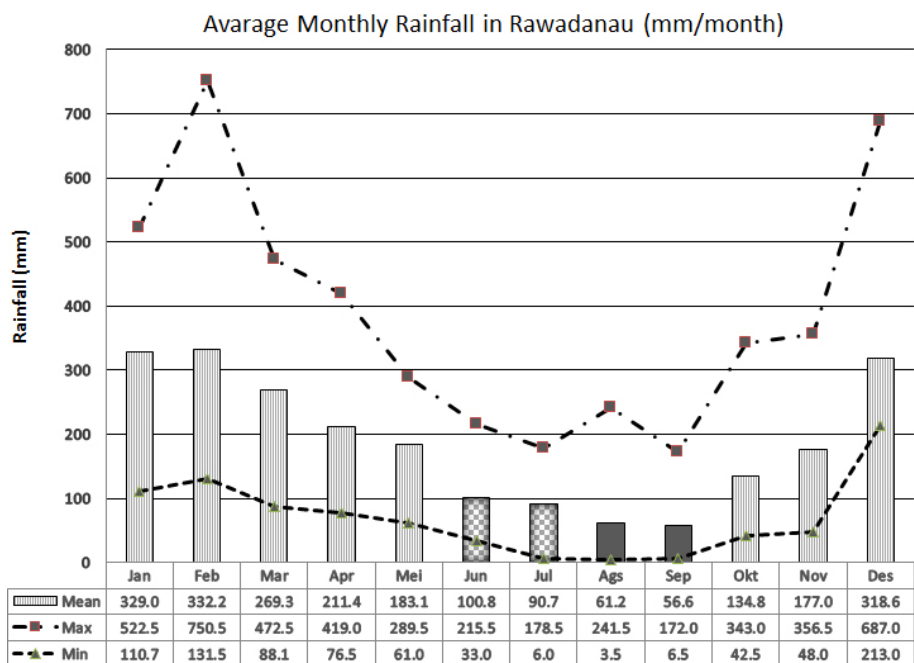|	Jan	Feb	Mar	Apr	Mei	Jun	Jul	Ags	Sep	Okt	Nov	Des
Mean	329.0	332.2	269.3	211.4	183.1	100.8	90.7	61.2	56.6	134.8	177.0	318.6
Max	522.5	750.5	472.5	419.0	289.5	215.5	178.5	241.5	172.0	343.0	356.5	687.0
Min	110.7	131.5	88.1	76.5	61.0	33.0	6.0	3.5	6.5	42.5	48.0	213.0

Figure 4: Average Monthly Rainfall in Rawadanau (mm/month).

2.1. Area description

2.1.1. Location

Rawadanau is located on the west side of Java Island at a morphology between 100 to 1350 metres above sea level (asl) (see **Figure 2**), located in the Serang province of Banten Indonesia. The research area is located at coordinates between 06° 07` 10” - 06° 19` 10” S and 105° 51` 30” - 106° 03` 00” E. The Cidanau River is the main river in the research area and flows to the Sunda Strait.

Based on meteorological data between 1996 and 2014, the average annual rainfall is 2806 mm (**Hartanto et al., 2019**). Rainy days occur throughout the year, and above ten days/month occur between November and May, when the intensity of monthly rainfall is above 200 mm, except from May to October. Minimum rainy days, occurring less than five days occur in August and September (see **Figure 3**), with average monthly rainfall intensity of 61.2 mm/month and 56.6 mm/month, respectively. The average dry peak occurs from August to September (intensity 50 mm/month), while the peak rainy season is from De-

cember to February with an intensity above 300 mm/month (see **Figure 4**), respectively.

The southern side of the research area is Mount Parakasak (990 metres asl), Mount Karang (1739 metres asl), Mount Aseupan (1081 metres asl), the north side is Mount Gede (741 metres asl), and the east side is Mount Kupak (361 metres asl).

2.1.2. Geological and hydrogeological characteristics

Rawadanau Sub-basin covers approximately 375 km², with the constituent rocks being the products of Mount Garung and Karang-Pulosari Volcano and alluvium (**Alam et al., 2014; Mulyadi, 1985; Suryadarma and Fauzi, 1991**). Two fault systems control Rawadanau, namely the Garung and Wangun system. Both of them have the same straight line pattern, namely NW-SE with rocks consisting of porphyritic andesite, basaltic andesite, and andesite formed since the Pleistocene era (**Suryadarma and Fauzi, 1991**). The discovery of hot springs containing solfatara around Rawadanau, which are the slopes of Mount Karang-Pulosari and Mount Garung, shows the remnants of volcanic activity and geothermal manifestations (**Mulyadi, 1985**).

The study area is comprised of Rawadanau deposits (Qr), consisting of gravel, clay sand, mud, and pumice crust. Colluvium sediment (Qk) forms from ruins, talus, and the dumping of volcanic ruins. Coral volcanic rocks (Qvk), composed of volcanic breccia, lava, tuff, and

lava, are inseparable. Young volcanic rock deposits (Qhv) are composed of volcanic breccia, lava, tuff, lava flows, and other volcanic eruptions (Mount Aseupan, Mount Parakasak). Upper Banten tuff (Qvtb) consists of tuff, pumice tuff, sandy tuff (at the top) and crystal tuff, rocky pumice tuff, glass tuff, and clay tuff insert at the bottom. Young Lake Volcanic Rock Deposits (Qvd) are composed of lava flows composed of andesite or basalt flapping, volcanic breccia, and tuff. Lower Banten tuff (Qptb) is composed of breccias, agglomerates, pumice tuffs, lapilli tuffs, and sandy tuffs. Old Lake Volcanic Rocks (Qpd) are a form of lava flow composed of andesite or raised basalt, volcanic breccia, and tuff.

Based on hydrogeology (see **Figure 5**), the study area aquifers are divided into cleft flow aquifers and intergrain spaces, aquifers through fractures, channels, cavities, and small productive aquifers and rare groundwater areas. Discharge areas include active, productive aquifers (discharge more than 5 litres/second), medium productive aquifers (discharge less than 5 litres/second), and rare groundwater (**Suryaman, 1999**).
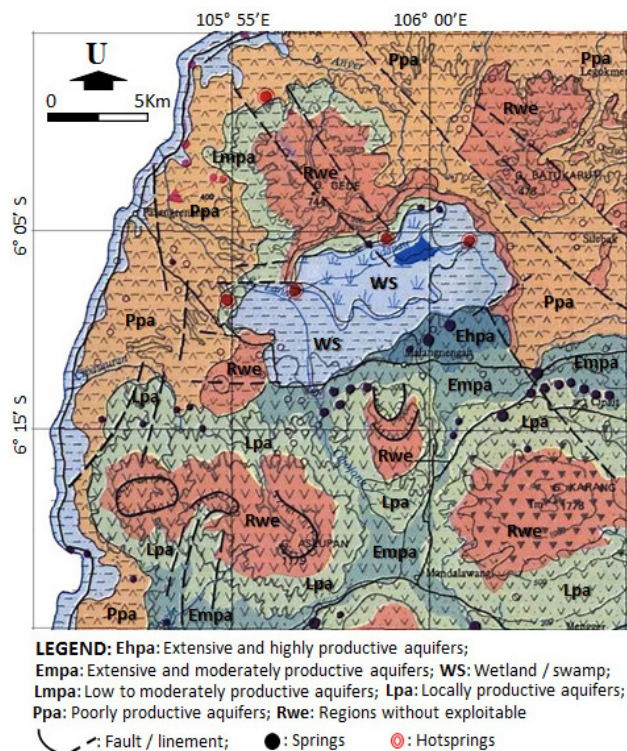
2.2. Water analysis

2.2.1. Water sampling and analysis

Water sampling was carried out at the peak of the dry season in September 2019. A set of 28 samples were taken, from wells, cold spring, rivers and hot springs. The 28 sample locations include seven rivers, five wells and 16 springs. Several water parameters were measured directly (in situ measure) using Water Checker Toac portable devices, including pH, temperature, and electrical conductivity (EC). All samples were put in 500 ml polyethylene bottles and analyzed for major ions (anions and cations) based on APHA 2005 at the Water Laboratory of the Research Center for Geotechnology - Indonesian Institute of Sciences (LIPI). Titrations analysis (Ca^{2+}, Mg^{2+}, HCO_3^-, and Cl^-), flame photometry (Na^+ and K^+), and spectrophotometry (for analysis of SO_4^{2-}, and SiO_2) were also undertaken. HCO_3^- analysis was carried out directly on the same day of collection, titrated using / with 0.01 or 0.1 M HCl against methyl orange and Bromocresol green indicators (**APHA, 2005**). The resulting analysis of the physical and chemical analyses are presented in **Table 1**. Minimum raw elements were analyzed to assess drinking water suitability (**Appelo and Postma, 2005**). The accuracy of the chemical analysis of water was verified by calculating the electrical balance (EB) where the error is generally less than about 5% with the equation:

$$\%EB = \frac{\sum Cations - \sum Anions}{\sum Cations + \sum Anions} X 100 \qquad (1)$$

Where $\sum$Cations is total cations in meq/l, $\sum$Anions is total anions in meq/l. An error above 5% indicates that analytical procedures should be examined (**Appelo and Postma, 2005**).

LEGEND: Ehpa: Extensive and highly productive aquifers;
Empa: Extensive and moderately productive aquifers; **WS:** Wetland / swamp;
Lmpa: Low to moderately productive aquifers; **Lpa:** Locally productive aquifers;
Ppa: Poorly productive aquifers; **Rwe:** Regions without exploitable
⌄: Fault / linement; ●: Springs; ◎: Hotsprings

Figure 5: Hydrogeology map of the study area (modified from Suryaman, 1999)

Table 1: The chemical components of the samples R = river; S = spring; W = well; σ = EB (electrical-balance)
(Hartanto et al., 2019)

ID	T	pH	EC	TDS	Na	K	Ca	Mg	HCO₃	CO₃	Cl	SO₄	SiO₂	σ
	(°C)		(µS/cm)	(mg/L)										
1R	27.7	7.65	222	144.30	18.02	4.57	18.40	5.84	97.50	0	27.55	3.36	54.59	-3.08
2R	26.2	7.11	64	41.60	8.12	2.72	8.00	2.95	52.70	0	8.26	2.16	37.58	-3.51
3W	26.8	6.16	262	170.30	9.79	0.56	28.40	9.00	139.66	0	17.91	3.147	39.91	-4.80
4W	29.7	6.00	269	174.85	11.61	1.24	26.80	5.59	92.23	0	28.92	11.666	34.24	-4.81
5W	27.7	6.69	473	307.45	16.13	6.94	57.20	8.27	208.18	0	34.44	14.895	46.59	-3.08
6S	30.4	6.49	210	136.50	7.49	4.36	30.20	10.30	115.95	0	37.19	2.275	94.32	-3.54
7S	42.6	6.75	1240	806.00	32.18	15.42	30.00	20.67	191.06	0	80.00	2.525	119.36	-4.30
8S	23.6	6.50	187	121.55	5.87	3.55	18.80	8.32	110.68	0	11.02	2.356	91.65	-4.94
10S	29.5	6.43	221	143.65	6.95	4.57	22.20	8.27	123.85	0	12.40	2.587	97.33	-4.87
11S	44.0	6.78	1298	843.70	54.18	32.24	70.20	36.97	405.82	0	123.00	2.169	126.70	-2.21
12S	41.4	6.88	1760	1144.00	60.69	56.61	74.80	69.18	585.01	0	179.00	2.284	128.37	-4.16
13S	41.3	6.62	2410	1566.50	86.70	42.99	102.80	86.67	624.68	0	298.00	2.649	124.03	-4.37
14W	27.2	6.76	505	328.25	12.62	6.74	49.00	21.38	213.35	0	63.36	3.538	65.61	-4.21
15R	29.2	6.93	239	155.35	6.95	4.50	24.20	7.84	100.14	0	27.55	2.809	64.61	-4.36
16W	30.5	6.69	612	397.80	38.65	18.12	62.20	46.83	542.99	0	38.57	3.111	85.64	-4.96
17W	31.2	6.63	1576	1024.40	60.07	16.57	70.60	64.10	373.32	41.46	192.00	2.854	99.66	-4.60
19R	23.5	7.56	97	63.05	1.14	1.51	16.20	4.40	65.88	0	8.26	2.064	53.59	-3.69
20S	25.1	5.95	116	75.40	2.10	2.94	16.40	4.65	68.51	0	11.02	2.516	52.60	-4.17
21R	25.0	7.10	73	47.45	1.69	1.65	11.40	3.68	47.43	0	8.26	2.275	52.93	-3.46
22S	25.3	6.11	46	29.90	1.25	1.11	9.40	2.46	34.26	0	6.89	2.364	40.25	-3.27
23S	27.6	6.55	140	91.00	2.77	2.80	10.80	5.35	45.26	0	9.64	2.96	75.96	4.28
24R	27.7	7.21	141	91.65	2.50	2.60	15.80	6.11	79.06	5.18	8.26	3.209	66.28	-9.34
25S	27.7	5.70	169	109.79	5.07	6.94	15.20	4.16	60.61	0	16.53	8.412	70.96	-4.34
26S	27.9	5.84	170	110.50	4.13	3.89	17.20	5.86	73.66	7.78	8.26	3.583	92.65	-4.55
27S	25.8	6.22	151	98.15	3.31	3.35	15.60	5.86	61.15	6.78	11.02	5.006	78.63	-4.87
28R	29.7	7.61	159	103.35	3.72	2.53	13.60	5.86	57.88	4.18	11.02	5.957	54.27	-4.65
29S	49.1	7.27	1155	750.75	36.62	25.94	55.80	28.46	288.39	31.21	68.87	14.21	145.07	-4.05
31S	49.7	6.32	2790	1813.50	212.25	102.43	116.80	78.64	214.60	32.58	771.00	9.683	152.73	-4.74
33S	51.8	6.48	2850	1852.50	147.83	67.32	70.60	40.24	232.58	58.86	376.00	6.251	157.07	-4.84

For isotope analysis (^{18}O and ^{2}H), the sample was put in a 100 ml polyethylene bottle analyzed at the Hydrochemical Laboratory of the Center for Groundwater and Environmental Geology, the Geological Agency of Indonesia using the Picarro L-2130-i analyzer. The results of the stable isotope analysis (^{18}O and ^{2}H) are presented in **Table 2**.

The TDS value is considered an essential value in determining water use and describing inorganic salts' presence and correlates with EC (**Logeshkumaran et al., 2015; Rusydi, 2018**). In this study, the TDS value is not measured directly, because this parameter is correlated with EC, usually expressed by a simple equation (**Clark and Fritz, 2013; Rusydi, 2018**):

$$TDS \ (mg/L) = 0.65 * EC \ (\mu S/cm) \qquad (2)$$

The interpretation of water types based on major ions is plotted in two basic triangles as the percentage of cations and milliequivalent anions of water chemistry using the Piper Diagram (**Piper, 1944**). Groundwater's hydrochemical characteristics, and correlation methods were used for the hydrochemical properties and the piper diagram (**Mirčovski et al., 2018**). The Gibbs Diagram was used to better understand the processes that occur during groundwater flowing and mechanisms for hydrochemical formation, (**Chintalapudi et al., 2016; Gibbs, 1970; Marandi and Shand, 2018**). To process statistical data SPSS V26 was used to process statistical data.

2.2.2. Statistical analysis

Statistical analysis was performed on the data from the analysis of water chemistry and stable isotopes. The

Table 2: The stable isotopes composition of the samples, R = river; S = spring; W = well

ID	δ¹⁸O	SD¹⁸O	δ²H	SD²H		ID	δ¹⁸O	SD¹⁸O	δ²H	SD²H
	(‰)						(‰)			
1R	-4.821	0.246	-31.302	0.639		17W	-5.946	0.249	-37.833	0.620
2R	-5.594	0.242	-36.894	0.650		19R	-5.936	0.252	-38.635	0.677
3W	-5.227	0.238	-34.200	0.616		20S	-6.370	0.236	-41.346	0.697
4W	-5.186	0.246	-33.778	0.629		21R	-4.955	0.242	-34.733	0.654
5W	-5.129	0.230	-33.832	0.621		22S	-5.803	0.235	-38.001	0.659
6S	-6.368	0.234	-40.680	0.668		23S	-6.052	0.240	-38.903	0.708
7S	-6.346	0.255	-40.644	0.697		24R	-5.864	0.229	-39.087	0.656
8S	-6.363	0.254	-41.025	0.723		25S	-5.920	0.249	-39.236	0.636
10S	-6.393	0.239	-40.970	0.660		26S	-6.115	0.242	-39.966	0.653
11S	-6.070	0.249	-39.648	0.659		27S	-5.684	0.239	-36.497	0.799
12S	-6.256	0.241	-40.138	0.636		28R	-4.999	0.241	-33.350	0.673
13S	-6.163	0.242	-40.500	0.634		29S	-5.851	0.246	-37.574	0.658
14W	-2.306	0.248	-19.063	0.697		31S	-5.863	0.254	-38.617	0.698
15R	-4.911	0.241	-32.765	0.757		33S	-5.989	0.233	-38.841	0.711
16W	-5.486	0.268	-35.094	0.756						

first step is to perform clustering based on the stable isotopes δ^2H and $\delta^{18}O$ (see **Figure 6**). Some of the water's chemical properties are related to each other, as indicated by the value of r (Pearson's correlation coefficient) with a value above 0.6 (**Marsal, 1987**). From the clustering results, the descriptive statistics and the correlation of each element were analyzed. The statistical analysis of all physical and chemical parameters, including minimum, maximum, mean, standard deviation, are presented in **Table 3**.

The main water elements can be easily determined using a box plot diagram (**Boateng et al., 2016; Srinivasamoorthy et al., 2014; Tizro and Voudouris, 2008**). The large concentration range of elemental content against standard deviation shows that the chemical composition of groundwater has been influenced by processes including water-rock interactions and anthropogenic influences (**Boateng et al., 2016; Srinivasamoorthy et al., 2014**). An increase in the main water element concentration is illustrated in the box plot diagram (see **Figure 7**). The box plot shows the upper and lower quartiles; the maximum and minimum values are shown as lines. The abundance of the main elements of anions in water is $HCO_3^- > Cl^- > SO_4^{2-} > CO_3^-$ and the cations is $Ca^{2+} > Na^+ > Mg^{2+} > K^+$, respectively.

3. Results

3.1. Hydrochemical characteristics

The hydrochemical analysis results, univariate of each cluster are shown in **Table 1** and **Table 3**. The primary ions value a charge balance error in water, from -4.96 to -2.21, while the mean error is -4.05. The error
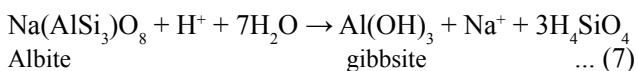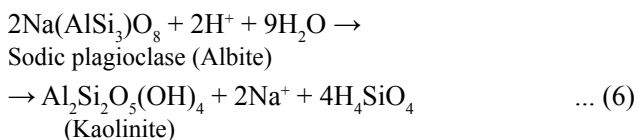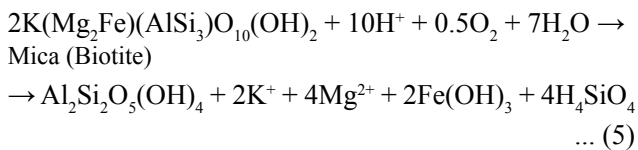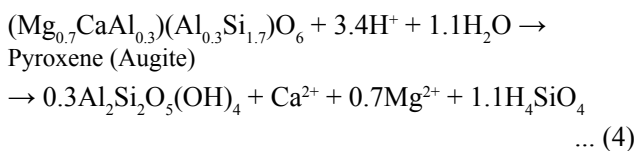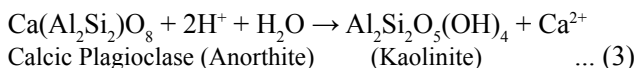
level shows that the analysis data meets the requirements, i.e., less than 5% (**Appelo and Postma, 2005**), to be used for further analysis.

The groundwater pH study area generally ranged from 5.7 to 7.7. Sub-cluster K1 had an average pH of 6.5, Sub-cluster K2 had an average pH of 6.7, and Cluster L had an average pH of 6.9, respectively. Water temperature ranged from 23.5 to 51.8°C (mean 32.1°C), sub-cluster K1 average temperature of 34.0°C, sub-cluster K2 averages 33.2°C, and cluster L averages 28.3°C, respectively. Hot springs were found in sub-clusters K2 and K1. At Batukuwung spring (near location 29S), the water temperature reached 65°C (**Hochstein and Sudarman, 2008**). More than 37.8°C can classify as hot springs (**Alfaro and Wallace, 1994**). Even if the water temperature is more than the average surface temperature in general or more than 36.7°C, it can be said to be hot springs (**Pentecost et al., 2003**).

The electrical conductivity (EC) Sub-cluster K1 ranged from 75 to 2410 µS/cm (mean 845.8 µS/cm), Sub-cluster K2 from 46 to 2850 µS/cm (mean 834.4 µS/cm), Cluster L was between 73 and 612 µS/cm (mean EC 73 µS / cm), respectively. This indicates that the groundwater has low salinity properties. An increase in the TDS value followed by an increase in the EC value was caused by the dissolving process that occurs when water flows due to evaporation, ion exchange resulting in an increasing concentration (**Delinom, 2009; Liu et al., 2015; Tóth, 1999**). For sub-cluster K1 and sub-cluster K2, respectively, the mean EC values of 845.5 µS/cm and 834.4 µS/cm, respectively, indicate that the existing groundwater contains many rock dissolved minerals. TDS value is considered an important value in determining water use. Total dissolved solids concentration

(TDS) ranged from 46.0 to 1852.5 mg/L, TDS sub-cluster K1 ranged from 75.4 to 1566.5 mg/L (mean 549.8 mg/L), sub-cluster K2 ranged from 29.9 to 1852.5 mg/L (mean 542.4 mg/L) and cluster L between 47.5 and 397.8 mg/L (mean 187.6 mg/L), respectively.

An abundance of the main element cation (see **Figure 7** and **Table 3**) is $Ca^{2+} > Na^+ > Mg^{2+} > K^+$. In general, content of the sequential cations were Ca^{2+} (between 8.0 and 116.8 mg/L) > Na^+ (1.1 to 212.3 mg/L) > Mg^{2+} (2.5 to 86.7 mg/L) > K^+ (0.6 to 102.4 mg/L), respectively. The Ca^{2+} content of the K1 sub-cluster ranged from 16.4 to 102.8 mg/L (mean 42.5 mg/L), the K2 sub-cluster ranged from 8.0 to 116.8 mg/L (mean 36.8 mg/L) and cluster L ranged from 11.4 to 62.2 mg/L (mean 30.3 mg/L). The high Ca^{2+} content is caused by enrichment due to the dissolution of Ca-plagioclase minerals (**Equation 3, 4** and **5**) (**Alam et al., 2014; Appelo and Postma, 2005**). The content of Mg^{2+} sub-cluster K1 ranged from 4.6 to 86.7 mg/L (mean 27.9 mg/L), sub-cluster K2 ranged from 2.5 to 78.6 mg/L (mean 22.1 mg/L) and cluster L ranged from 3.7 to 46.8 mg/L (mean 11.6 mg/L), respectively. Rocks composed of tuff caused high Mg^{2+} content. The groundwater passed through aquifers composed of tuffs and andesitic rocks. The formation of secondary clay minerals resulting from the dissolution of silicate minerals such as albite produces clay minerals such as kaolinite, which can enrich minerals in groundwater system as shown in the following equations (**Equation 3, 4, 5, 6** and **7**) (**Appelo and Postma, 2005**):

$$Ca(Al_2Si_2)O_8 + 2H^+ + H_2O \rightarrow Al_2Si_2O_5(OH)_4 + Ca^{2+}$$
Calcic Plagioclase (Anorthite)   (Kaolinite)   ... (3)

$$(Mg_{0.7}CaAl_{0.3})(Al_{0.3}Si_{1.7})O_6 + 3.4H^+ + 1.1H_2O \rightarrow$$
Pyroxene (Augite)

$$\rightarrow 0.3Al_2Si_2O_5(OH)_4 + Ca^{2+} + 0.7Mg^{2+} + 1.1H_4SiO_4$$
... (4)

$$2K(Mg_2Fe)(AlSi_3)O_{10}(OH)_2 + 10H^+ + 0.5O_2 + 7H_2O \rightarrow$$
Mica (Biotite)

$$\rightarrow Al_2Si_2O_5(OH)_4 + 2K^+ + 4Mg^{2+} + 2Fe(OH)_3 + 4H_4SiO_4$$
... (5)

$$2Na(AlSi_3)O_8 + 2H^+ + 9H_2O \rightarrow$$
Sodic plagioclase (Albite)

$$\rightarrow Al_2Si_2O_5(OH)_4 + 2Na^+ + 4H_4SiO_4$$ ... (6)
(Kaolinite)

$$Na(AlSi_3)O_8 + H^+ + 7H_2O \rightarrow Al(OH)_3 + Na^+ + 3H_4SiO_4$$
Albite   gibbsite   ... (7)

The Na^+ content of the K1 sub-cluster ranged from 2.1 to 86.7 mg/L (mean 28.9 mg/L), the K2 sub-cluster ranged from 1.1 to 212.2 mg/L (mean 43.7 mg/L) and cluster L ranged from 1.7 to 38.7 mg/L (mean 13.3
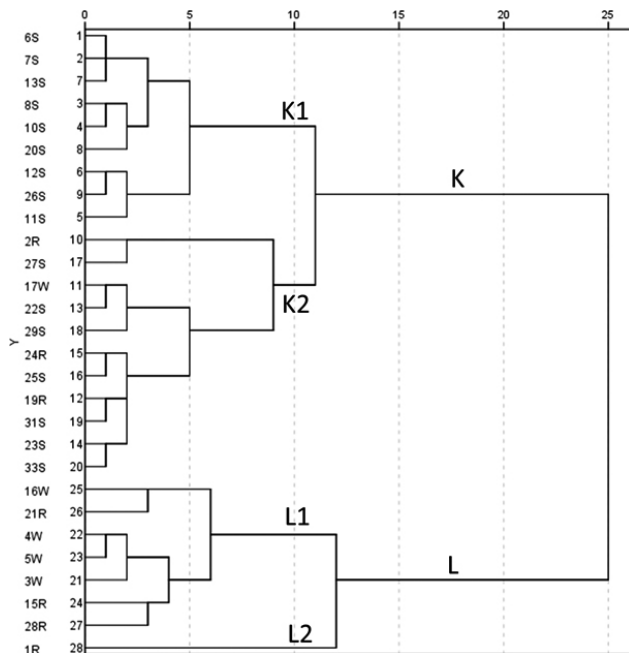
Figure 6: Dendrogram results from hierarchical cluster analysis using d¹⁸O and d²H

mg/L), respectively. Some locations where very high Na^+ content (31S and 33S) was found are thought to be formation water. The K^+ content K1 sub-cluster ranged from 2.9 to 56.6 mg/L (mean 18.5 mg/L), the K2 sub-cluster ranged from 1.1 to 102.4 mg/L (mean 21.2 mg/L) and the L cluster ranged from 0.6 to 18.1 mg/L (mean 5.0 mg/L), respectively. The presence of K^+ in water results from dissolving igneous rock minerals (**Equation 5**) (**Appelo and Postma, 2005**).

The presence of the main elements of anions in water (see **Figure 7** and **Table 3**) is $HCO_3^- > Cl^- > SO_4^{2-} > CO_3^-$. HCO_3^- (between 34.3 and 624.7 mg/L) > Cl^- (between 6.9 and 771.0 mg/L) > SO_4^{2-} (between 2.1 and 14.90 mg/L) > CO_3^- (between 0.0 and 58.9 mg/L), respectively. The HCO_3^- content - sub-cluster K1 ranged
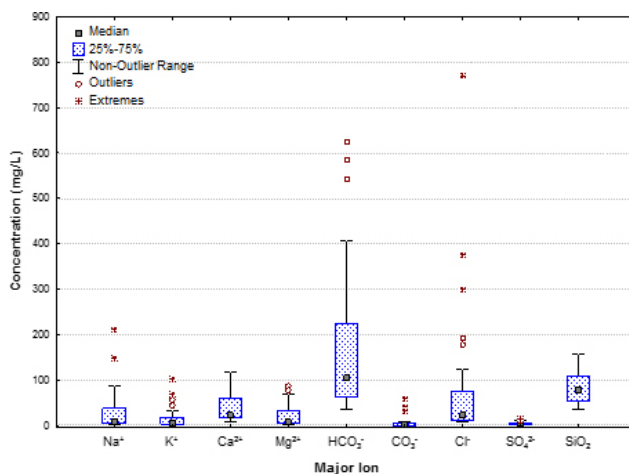
Figure 7: Box and whisker plot of major ions in groundwater samples. The stars represent extremes and white circles represent outliers

Table 3: Univariate statistical overview of the data set. All values are in mg/L unless otherwise indicated.
S.Dev. = Standard deviation. W = well; S = spring; and R = river. TDS and concentration of ions are in mg/L unit

Cluster	ID	Value	T (°C)	pH	EC (µS/cm)	TDS (calc)	Na⁺	K⁺	Ca²⁺	Mg²⁺	HCO₃⁻	CO₃⁻	Cl⁻	SO₄²⁻	SiO₂
K1	6S, 7S, 13S, 8S, 10S, 20S, 12S, 26S, 11S	Max	44.0	6.9	2410.0	1566.5	86.7	56.6	102.8	86.7	624.7	7.8	298.0	3.6	128.4
		Min	23.6	5.8	116.0	75.4	2.1	2.9	16.4	4.6	68.5	0.0	8.3	2.2	52.6
		Mean	34.0	6.5	845.8	549.8	28.9	18.5	42.5	27.9	255.5	0.9	84.4	2.5	103.0
		S.Dev	8.2	0.4	855.9	556.3	31.2	20.4	31.7	30.4	222.9	2.6	100.0	0.4	24.5
K2	2R, 27S, 17W, 22S, 29S, 24R, 25S, 19R, 31S, 23S, 33S	Max	51.8	7.6	2850.0	1852.5	212.2	102.4	116.8	78.6	373.3	58.9	771.0	14.2	157.1
		Min	23.5	5.7	46.0	29.9	1.1	1.1	8.0	2.5	34.3	0.0	6.9	2.1	37.6
		Mean	33.2	6.7	834.4	542.4	43.7	21.2	36.8	22.1	137.1	16.0	134.2	5.4	88.9
		S.Dev	11.1	0.6	1103.2	717.1	71.4	33.3	36.2	27.4	118.3	21.2	240.8	3.9	44.0
L	16W, 21R, 3W, 4W, 5W, 15R, 28R, 1R	Max	30.5	7.7	612.0	397.8	38.7	18.1	62.2	46.8	543.0	4.2	38.6	14.9	85.6
		Min	25.0	6.0	73.0	47.5	1.7	0.6	11.4	3.7	47.4	0.0	8.3	2.3	34.2
		Mean	28.3	6.9	288.6	187.6	13.3	5.0	30.3	11.6	160.8	0.5	24.3	5.9	54.1
		S.Dev	1.8	0.6	173.1	112.5	11.7	5.7	19.2	14.3	162.4	1.5	10.8	4.8	15.9
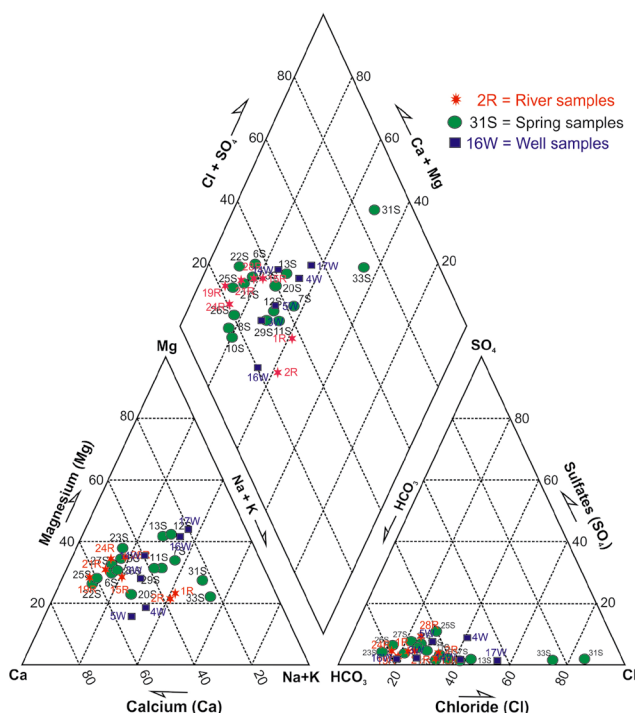
Figure 8: Piper diagram for hydrochemical types of Rawadanau. All data in meq/L normalized to 100% (**Hartanto et al., 2019**)

from 68.5 to 624.7 mg/L (mean 255.5 mg/L), sub-cluster K2 ranged from 34.3 to 373.3 mg/L (mean 137.1 mg/L) and cluster L ranged from 47.4 to 543.0 mg/L (mean 160.8 mg/L), respectively. The presence of carbonates and bicarbonates as dissolution of the remaining carbonate minerals commonly contained in igneous rocks (**Appelo and Postma, 2005**).

Carbonate (CO_3^-) was generally only detected at the K2 sub-cluster between 0.0 and 58.9 mg/L (mean 16.0 mg/L), and in the K1 sub-cluster, only one location (26S) had a value of 7.8 mg/L and one location in the L cluster (28R) of 4.2 mg/L. The chloride content of the K1 sub-cluster was 8.3 to 298.0 mg/L (mean 84.4 mg/L), the K2 sub-cluster was between 6.9 to 771.0 mg/L (mean 134.2 mg/L), and the L cluster between 8.3 to 38.6 mg/L (24.3 mg/L), respectively. Likewise, the high Na⁺ content, followed by the high Cl⁻ content in several locations, is probably sourced from formation water flowing at hot springs (13S, 31S, and 33S).

The sulfate (SO_4^{2-}) content of the K1 sub-cluster ranged from 2.2 to 3.6 mg/L (mean 2.5 mg/L), the K2 sub-cluster ranged from 2.1 to 14.2 mg/L (mean 5.4 mg/L) and the L cluster ranged from 2.3 to 14.9 mg/L (mean 5.9 mg/L), respectively. The low SO_4^{2-} content proves that the study area's water source has not been contaminated by anthropogenic factors or mineral dissolution, rich in sulfates. Low-sulfate groundwater is pristine freshwater (**Appelo and Postma, 2005**).

In September, during the peak dry season, silica (SiO_2) in groundwater varied from 34.24 mg/L to 157.07 mg/L. SiO_2 content was found in all clusters, SiO_2 in the sub-cluster K1 was between 52.6 to 128.4 mg/L (mean 103.0 mg/L), in the K2 sub-cluster between 37.6 to 157.1 mg/L (mean 88.9 mg/L), and in cluster L between 34.2 to 85.6 mg/L (mean 54.1 mg/L), respectively. The presence of silica indicates the dissolution of rock constituent minerals, which are usually closely related to geothermal source (**Giggenbach, 1981**).

The results plotted on a piper diagram yield two dominant water types: Ca-Mg-HCO₃-Cl and Ca-Mg-HCO₃.

Table 4: Correlations coefficient of major parameters and isotopes in groundwater (bold shows a strong correlation)

	T	pH	EC	TDS	Na	K	Ca	Mg	HCO$_3$	CO$_3$	Cl	SO$_4$	SiO$_2$	δ^{18}O	δ^{2}H
T	1.00														
pH	0.06	1.00													
EC	**0.89**	-0.02	1.00												
TDS	**0.89**	-0.02	*1.00*	1.00											
Na	**0.81**	-0.07	**0.93**	**0.93**	1.00										
K	**0.85**	-0.05	**0.92**	**0.92**	**0.97**	1.00									
Ca	**0.78**	-0.03	**0.91**	**0.91**	**0.86**	**0.86**	1.00								
Mg	**0.70**	0.00	**0.89**	**0.89**	**0.80**	**0.82**	**0.94**	1.00							
HCO$_3$	0.57	0.08	**0.68**	**0.68**	0.49	0.56	**0.81**	**0.86**	1.00						
CO$_3$	**0.62**	-0.02	**0.67**	**0.67**	**0.69**	**0.60**	0.50	0.45	0.18	1.00					
Cl	**0.73**	-0.10	**0.88**	**0.88**	**0.98**	**0.94**	**0.83**	**0.78**	0.41	**0.62**	1.00				
SO$_4$	0.31	-0.10	0.18	0.18	0.23	0.22	0.27	0.03	-0.02	0.32	0.22	1.00			
SiO$_2$	**0.88**	-0.03	**0.83**	**0.83**	**0.74**	**0.79**	**0.73**	**0.72**	**0.59**	**0.60**	**0.68**	0.10	1.00		
δ^{18}O	-0.27	0.36	-0.28	-0.28	-0.18	-0.25	-0.19	-0.28	-0.23	-0.12	-0.18	0.28	**-0.54**	1.00	
δ^{2}H	-0.25	0.36	-0.27	-0.27	-0.18	-0.25	-0.17	-0.26	-0.18	-0.09	-0.20	0.30	**-0.52**	**0.98**	1.00

Two locations (31S and 33S) were showing the Na-Cl type (see **Figure 8**). The sodium chloride types of water (31S and 33S) are likely formed due to groundwater interaction with magmatic rock with minerals containing sodium and chlorine (**Mirčovski et al., 2018**). Calcium-magnesium bicarbonate facies reflects the geology and climate of the study area. Besides, the research area is composed of volcanic rock products, so the groundwater interacts with mineral compounds in the aquifer between the groundwater and the rocks it passes through (**Alam et al., 2014**). Ion exchange occurs between Na$^+$ + K$^+$ ions in water and soil Ca^{2+} and Mg^{2+} during the long water's residence time in the rock (**Equation 3, 4, 5, 6** and **7**). Several locations show a high Cl$^-$ content; this indicates that water has travelled relatively far from its source, thus experiencing enrichment of mineral chloride due to mineral dissolution and ancient salt. In general, the longer the groundwater remains in contact with the aquifer rocks, the greater the material it will take into solution, the chemical evolution of groundwater tends toward seawater's chemical composition (**Chebotarev, 1955**).

3.2. Correlation analysis

Several chemical properties of water are related to each other (**Marsal, 1987**). Pearson's correlation coefficient is used to measure and find the strength of any linear relationship between two numerical variables. The results of the correlation matrix between 17 chemical water parameters are calculated and presented in **Table 4**. Pearson's correlation coefficient values range between +1 and -1, where values close to 0.00 do not indicate a linear relationship (**Tabachnick and Fidell, 2013**). An r value of +1.00 or -1.00 indicates one of perfect predictability when the other is known. Based on Pearson's correlation, the positive correlation is significant and high (r > 0.7).

As in **Table 4**, a positive, robust, and consistent correlation is shown by temperature and EC with almost all variables from the correlation test result. In addition, a powerful correlation was shown by sodium with potassium, calcium, magnesium and chloride (r = 0.80 - 0.98), between potassium and calcium, magnesium, chloride (r = 0.82 - 0.94), between calcium and magnesium, bicarbonate, chloride (r = 0.81 - 0.94), between magnesium and bicarbonate (r = 0.86), respectively. The powerful and positive correlation between Ca^{2+}, Mg^{2+}, and Na$^+$ is probably a manifestation of the ion exchange process that has taken place during the dissolution of silicate minerals (**Equation 3, 4, 5, 6** and **7**) (**Adams et al., 2001; Zhang et al., 2018**). Strong correlation between sodium and carbonate (r = 0.69), potassium with carbonate (r = 0.60), magnesium with chloride (r = 0.78), carbonate with chloride (r = 0.62). The content of silica
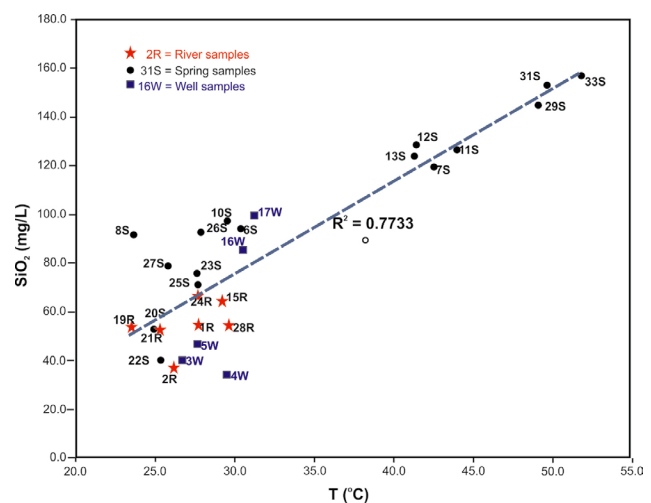
Figure 9: Relationship between SiO$_2$ and T (temperature) water samples in Rawadanau

(SiO_2) has a strong correlation with major ions (r = 0.60 - 0.79); this indicates that the dissolution of the minerals that make up the rock produces silica minerals, which are usually closely related to geothermal (**Giggenbach, 1981**). The correlation between SiO_2 and temperature can be seen in **Figure 9**.

Figure 9 shows an existing correlation between temperature (T) and silica (SiO_2); an increase in temperature will also offset the more effective SiO_2 content. This SiO_2 can be used as a reliable geothermometer guide in geothermal investigations (**Zhang et al., 2019**). The graph shows that springs have a temperature between 41.3 to 51.8°C (7S, 11S, 12S, 13S, 29S, 31S, 33S) with SiO_2 concentrations ranging from 119.4 to 157.1 mg/L. The increase in concentration mainly comes from dissolving rocks containing SiO_2 during groundwater circulation in the rock.

3.3. Water stable isotopes

A graph representing the relationship between $\delta^{18}O$ and δ^2H regarding the global meteoric water line is presented in **Figure 10**. The graph shows that the K1 sub-cluster and K2 sub-cluster are distributed adjacent to the global meteoric water line (GMWL) as described by **Craig (1961)**. The local water meteoric line in the study area refers to Jakarta's closest model (**Lubis et al., 2008**); the equation used is y = 8x + 10. Cluster L under GMWL shows that it has been heavily influenced by evaporation so that enrichment occurs. Cluster L is heavier than sub-clusters K1 and K2, and this indicates that the groundwater from sub-cluster K1 and sub-cluster K2 has interacted a lot with rocks on its way.

Cluster analysis is based on the dependence of several water quality parameters. This study was carried out with an approach based on the stable isotope content ($\delta^{18}O$ and δ^2H) in water (see **Figure 6**). The use of stable isotopes ($\delta^{18}O$ and δ^2H) was considered because they are both durable and do not decay over a geological period (**Clark and Fritz, 2013; Liu et al., 2015; Tweed et al., 2019**). The dendrogram graph based on the stable isotopes δ^2H and $\delta^{18}O$ (see **Figure 6**) show two groups, namely cluster K 20 samples and L cluster 8 samples. Cluster K includes sub-cluster K1; there are 9 locations (6S, 7S, 8S, 10S, 11S, 12S, 13S, 20S, and 26S). The lightest isotope content of Sub-Cluster K1, maximum $\delta^{18}O$ and δ^2H (-6.1 ‰ and -39.6 ‰), minimum (-6.4 ‰ and -41.3 ‰), mean (-6.3 ‰ and - 40.5 ‰), respectively. The sample from the springs tends to be lighter so that the isotope content is depleted.

The K2 sub-cluster contains 11 samples 2R, 27S, 17W, 22S, 29S, 24R, 25S, 19R, 31S, 23S and 33S. The isotope content of the sub-Cluster K2 is generally heavier than the sub-cluster K1; the sample consists of springs, dug wells, and rivers. The full contents were δ^2H and $\delta^{18}O$ (-5.6 ‰ and -36.5 ‰), minimum (-6.1 ‰ and -39.2 ‰), with a mean (-5.9 ‰ and -38.2 ‰), respectively.

There are 8 locations: cluster L, including sub-cluster L1 (7 samples) and sub-cluster L-2 (1 sample), where dug wells and rivers dominate the water sources. Cluster L includes eight samples, consisting of wells and rivers covering 16W, 21R, 3W, 4W, 5W, 15R, 28R, and 1R. The full contents were δ^2H and $\delta^{18}O$ (-4.8 ‰ and -31.3 ‰), minimum (-5.5 ‰ and -35.1 ‰), with a mean (-5.1 ‰ and -33.6 ‰), respectively.

4. Discussion

4.1. Hydrochemical characteristics

The hydrochemical analysis result showed that groundwater pH ranged from 5.7 to 7.7; the water temperature was between 23.5 and 51.8°C. A water temperature of more than 36.7°C indicates hot springs (**Pentecost et al., 2003**). There was a water temperature of up to 51.8°C, which is more than 36.7°C, and silica (SiO_2) is found as an indication of a geothermal source (**Pentecost et al., 2003; Zhang et al., 2019**). Throughout the geothermal system, the processes that occur show that the dissolution of the minerals that make up the rock produces silica, which is the most stable mineral under a given set of conditions (**Giggenbach, 1981**). The hot springs (13S, 31S, and 33S) contain high levels of Na^+ and Cl^-, possibly from formation water that comes out as springs or as seawater trapped in aquifers (**Villegas et al., 2018**).

Hydrochemistry is influenced by the interaction between water and the medium in which it passes, in this case, rock, changes in water's chemical characteristics depending on the type of rock and the water composition. Water is predominantly bicarbonate (HCO_3^-), and the main cation is Ca^{2+}. According to the piper diagram (see **Figure 8**) of water types are generally Ca-HCO_3 and Mg-HCO_3. Water facies like this show that groundwater is still relatively pristine, originating from rainwater. The study area is primarily composed of volcanic products, mainly tuff, porphyritic andesite, basaltic andesite, and andesite, rich in plagioclase. The groundwater flow occurs mineral dissolution, resulting in mineral enrichment in aquifers' groundwater (**Alam et al., 2014**). According to the piper diagram (see **Figure 8**), the SO_4^{2-} content is relatively low, not more than 14.9 mg/L, proving that groundwater is freshwater that is still original (**Appelo and Postma, 2005**). The SO_4^{2-} is related to pesticides or fertilizers, besides dissolution minerals as gypsum and seawater related (**Villegas et al., 2018**).

4.2. Groundwater isotope characteristics

The study area's local meteoric water line refers to the nearest meteoric, namely GMWL Jakarta (**Lubis et al., 2008**), the equation used is y = 8x + 10. Plotting the relationship between δ^2H and $\delta^{18}O$ (see **Figure 10**) has at least two patterns: a) coincide with the GMWL, which is occupied by the K-1 and K-2 sub-clusters; b) the pattern
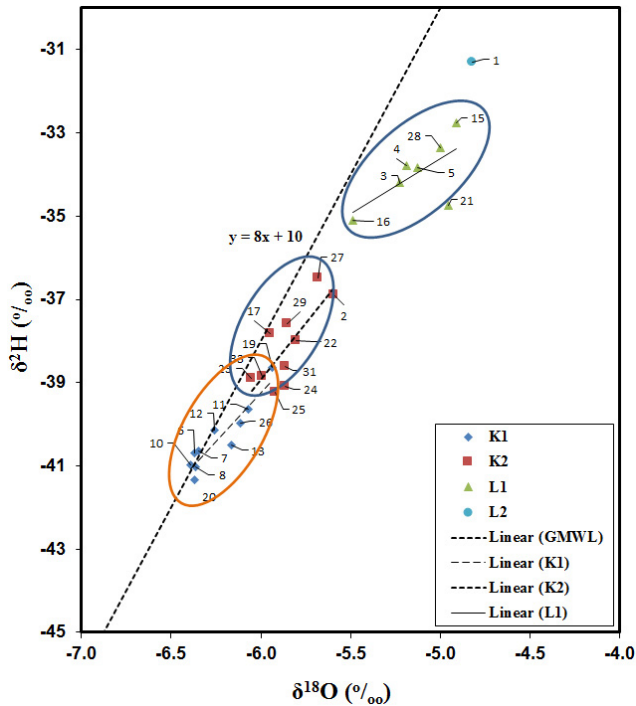
Figure 10: Relationship between hydrogen (d²H) and oxygen (d¹⁸O) isotopes of groundwater samples in Rawadanau

that tends to move away from the GMWL is occupied by the L sub-cluster. The K-1 and K2 sub-clusters almost coincide with the GMWL, indicating that the groundwater is affected by local climate and local topography (**Lee et al., 1999**).

Dendrogram graph analysis based on the stable isotopes $\delta^{18}O$ and δ^2H (see **Figure 6**) produces two groups: K of 20 sites, and L of 8 sites. Sub-Cluster K1 includes location of cold-springs (6S, 8S, 10S, 20S, and 26S) and hot-springs (7S, 11S, 12S, 13S), with mean isotope content of $\delta^{18}O$ and δ^2H are -6.3 ‰ and - 40.5 ‰, respectively. Sub-Cluster K2 average isotope content of river water samples (2R, 24R, 19R), well (17W), cold springs (27S, 22S, 25S, 23S) and hot-springs (29S, 31S, 33S), of $\delta^{18}O$ and δ^2H are -5.9 ‰ and - 38.2 ‰, respectively. Cluster L includes sub-sub-clusters L1 (7 locations) of dug well (3W, 4W, 5W, 16W) and river water (21R, 15R, 28R) and sub-cluster L-2 (1R). The mean content $\delta^{18}O$ and δ^2H are -5.1 ‰ and - 33.6 ‰, respectively. At four locations, namely the river water (1R, 15R, 21R, and 28R), stable isotope content indicates evaporated water.

Although the type of water is relatively the same, dominated by springs, the isotope content of the sub-Cluster K2 is generally heavier than the sub-Cluster K1. The isotope content (δ^2H and $\delta^{18}O$) of the K1 sub-Cluster is more depleted and lighter than others (K2, L1, and L2), indicating that these samples are characterized by water with a longer residence time in the aquifer. Furthermore, the same kind of water is from river water; the sub-Cluster K2 contents isotope is lighter than the sub-cluster L.
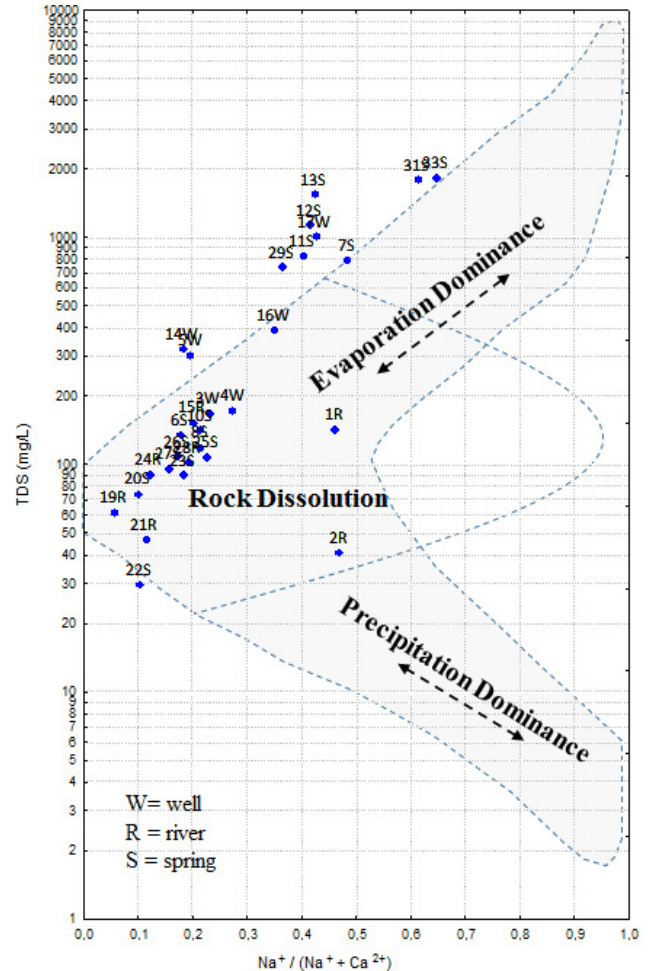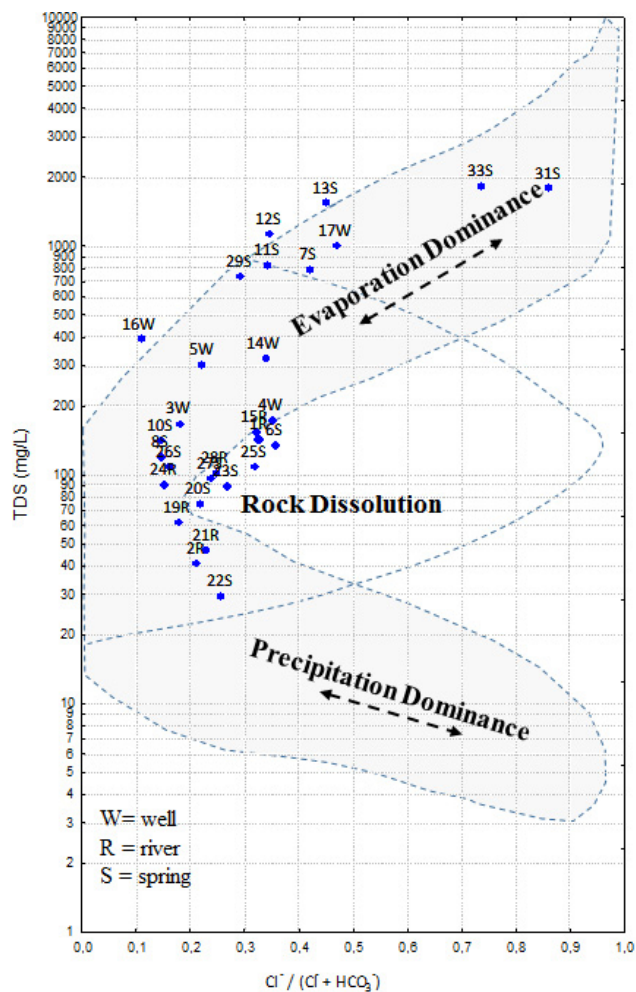

Figure 11: Gibbs diagram of groundwater samples in Rawadanau: TDS vs. Na⁺ / (Na⁺ + Ca²⁺)

4.3. Groundwater interactions

Studying the mechanism of groundwater evolution, **Gibbs (1970)** provided a simple solution by making a semi-logarithmic graph of the relationship between TDS versus the ratio of $Na^+ / (Na^+ + Ca^{2+})$ and $Cl^- / (Cl^- + HCO_3^-)$. Three mechanisms form the graph: dominance of precipitation, dominance of rock dissolution processes, and evaporation dominance (**Gibbs, 1970; Srinivasamoorthy et al., 2014**).

Plotting the data on the Gibbs chart, which compares TDS with the ratio of $Cl^- / (Cl^- + HCO_3^-)$ and ratio of $Na^+ / (Na^+ + Ca^{2+})$ water, produces two groups, namely evaporation dominance, and rock dissolution processes dominance. Based on the Gibbs graph, which reflects the relationship between TDS and the $Na^+ / (Na^+ + Ca^{2+})$ ratio (see **Figure 11**), it is divided into two groups, namely evaporation dominance for the sub-cluster K1 (7S, 11S, 12S, 13S) and the sub-cluster K2 (17W, 29S, 31S, 33S) and rock dissolution dominance for the K1 sub-cluster (6S, 8S, 10S, 20S, 26S), the K2 sub-cluster (2R, 27S, 22S, 24R, 25S, 19R, 23S) all L cluster (16W, 21R, 3W, 4W, 5W, 15R, 28R, 1R), respectively.

Figure 12: Gibbs diagram of groundwater samples in Rawadanau: TDS vs. Cl⁻ / (Cl⁻ + HCO₃⁻)

According to **Figure 12**, the Gibbs chart shows the comparison between TDS and the ratio of Cl^- / (Cl^- + HCO_3^-), divided into two groups, i.e., evaporation dominance and rock dissolution dominance. Eight locations are the evaporation dominance group, including 7S, 11S, 12S, 13S, 17W, 29S, 31S, and 33S. Besides, locations 31S and 33S are rich in chloride (leading to saltwater). Meanwhile, they remain as the second group, i.e., dissolution rock, comprise river water, springs, and dug well. The rock dissolution includes K1 (five samples), and K2 (seven samples), and all L sub-clusters (six samples).

The results of plotting data on the Gibb chart (see **Figure 11** and **Figure 12**) through the TDS ratio of Na^+ / (Na^+ + Ca^{2+}) and Cl^- / (Cl^- + HCO_3^-) the ratio of are generally in the area of rock dissolution dominance and evaporation dominance (**Gibbs, 1970; Marandi and Shand, 2018; Srinivasamoorthy et al., 2014**). That indicates that there is an area of evaporation from several springs. Also, samples from river water, wells, and cold springs are heavily influenced by dissolution and weathering of the minerals that make up volcanic rocks from tuff and andesite, generally containing feldspar (**Alam et al., 2014; Appelo and Postma, 2005**).

5. Conclusions

Hydrochemical analysis has been performed to determine the quality, type, and dominant hydrochemical processes in the study area. The study examined groundwater origin in Rawadanau using a stable isotope approach (δ^2H and $\delta^{18}O$) and hydrochemical analyses. Groundwater quality was assessed by physical properties (pH, EC, temperature) and water chemistry (cations and anions). The pH was found to be between 5.6 to 7.7, except for the nearby hot springs, which are more acidic (pH 5.7 - 5.9). There are two sub-clusters of the grouping using stable isotopes: cluster K and cluster L. The isotope content (δ^2H and $\delta^{18}O$) of cluster K is lighter than the L cluster. According to stable isotope data (δ^2H and $\delta^{18}O$), groundwater that fills Rawadanau comes from meteoric water.

Meanwhile, the evaporation dominance and rock dissolution dominance factors have changed the groundwater, as shown in the Gibbs diagram. The effect of evaporation and interaction with a rock when groundwater flows cause depleted isotopes and various water types. The type of groundwater in Rawadanau is influenced by mineral dissolution and mineral content volcanic rocks, and this is in line with the evolutionary sequence of Chebotarev. The rocks are comprised of porphyritic andesite, basaltic andesite, and andesite. The chemical compositions are mainly affected by volcanic dissolution. The enrichment of weathered igneous rock products at peak dry season produces four types of groundwater. The Ca-HCO₃ type dominates river water and cold springs. Meanwhile, hot springs have three types of water: Mg-Ca-HCO₃-Cl, Ca-Mg-HCO₃, and Na-Cl.

6. References

Adams, S., Titus, R., Pietersen, K., Tredoux, G. and Harris, C. (2001): Hydrochemical characteristics of aquifers near Sutherland in the Western Karoo, South Africa. Journal of Hydrology, 241, 1–2, 91–103. https://doi.org/10.1016/S0022-1694(00)00370-X

Alam, B. Y. C. S. S. S., Itoi, R., Taguchi, S. and Yamashiro, R. (2014): Spatial Variation in Groundwater Types in the Mt. Karang (West Java, Indonesia) Volcanic Aquifer System Based on Hydro-Chemical and Stable Isotope ([delta] D and [delta]^ sup 18^ O) Analysis. Modern Applied Science, 8, 6, 87–102. https://doi.org/10.5539/mas.v8n6p87

Alfaro, C. and Wallace, M. (1994): Origin and classification of springs and historical review with current applications. Environmental Geology, 24(2), 112–124. https://doi.org/10.1007/BF00767884

APHA (2005): Standard Methods for the Examination of Water and Wastewater. 21st Ed. American Public Health Association, Washington DC, 1220p. https://doi.org/10.2105/SMWW.2882.216

Appelo, C. A. J. and Postma, D. (2005): Geochemistry, groundwater and pollution. 2nd. Ed. Balkema, Rotterdam, 634p.

Boateng, T. K., Opoku, F., Acquaah, S. O. and Akoto, O. (2016): Groundwater quality assessment using statistical approach and water quality index in Ejisu-Juaben Municipality, Ghana. Environmental Earth Sciences, 75, 6, 489. https://doi.org/10.1007/s12665-015-5105-0

Chebotarev, I.I (1955) Metamorphism of natural waters in the crust of weathering—1. Geochimica et Cosmochimica Acta, 8, 1-2: 22–48. https://doi.org/10.1016/0016-7037(55)90015-6

Chen, J., Liu, X., Wang, C., Rao, W., Tan, H., Dong, H., Sun, X., Wang, Y., and Su, Z. (2011): Isotopic constraints on the origin of groundwater in the Ordos Basin of northern China. Environmental Earth Sciences, 66, 505–517. https://doi.org/10.1007/s12665-011-1259-6

Chintalapudi, P., Pujari, P., Khadse, G., Sanam, R. and Labhasetwar, P. (2016): Groundwater quality assessment in emerging industrial cluster of alluvial aquifer near Jaipur, India. Environmental Earth Sciences, 76, 1, 8. https://doi.org/10.1007/s12665-016-6300-3

Clark, I. D. and Fritz, P. (2013): Environmental Isotopes in Hydrogeology. Lewis Publishers New York, 329 p.

Craig, H. (1961): Isotopic variations in meteoric waters. Science, 133, 3465, 1702–1703. https://doi.org/10.1126/science.133.3465.1702

Delinom, R. M. (2009): Structural geology controls on groundwater flow: Lembang Fault case study, West Java, Indonesia. Hydrogeology Journal, 17(4), 1011–1023. https://doi.org/10.1007/s10040-009-0453-z

Gibbs, R. J. (1970): Mechanisms controlling world water chemistry. Science, 170, 3962, 1088–1090. https://doi.org/10.1126/science.170.3962.1088

Giggenbach, W. F. (1981): Geothermal mineral equilibria. Geochimica et Cosmochimica Acta, 45, 3, 393–410. https://doi.org/10.1016/0016-7037(81)90248-9

Hartanto, P., Delinom, R. M. and Hendarmawan, H. (2019): Type and Quality of Water at the Peak of Dry Season Based on the Major Elements of Water Chemical at Rawa Danau Serang Regency. RISET Indonesian Journal of Geology and Mining, 29, 1, 13–25. (*In Indonesian, with English abstract*) https://doi.org/10.14203/risetgeotam2019.v29.1021

Hochstein, M. P. and Sudarman, S. (2008): History of geothermal exploration in Indonesia from 1970 to 2000. Geothermics, 37, 3, 220–266. https://doi.org/10.1016/j.geothermics.2008.01.001

Houria,B., Mahdi, K., and Zohra, T.T. (2020): Hydrochemical Characterisation of Groundwater Quality: Merdja Plain (Tebessa Town, Algeria), Civil Engineering Journal, Vol. 6, No. 2, February, 2020. http://dx.doi.org/10.28991/cej-2020-03091473

Hussain, M.R and Abed, B. Sh (2019): Simulation and Assessment of Groundwater for Domestic and Irrigation Uses, Civil Engineering Journal, Vol. 5, No. 9, September, 2019. http://dx.doi.org/10.28991/cej-2019-03091379

KEMEN-ESDM. (2017): Regulation of The Minister of Energy and Mineral Resources of The Republic of Indonesia, Number 2 of 2017 Concering the Groundwater Basin in Indonesia, Ministry of Energy and Mineral Resources. Jakarta, 102p. (*Peraturan Menteri ESDM No. 2 Tahun 2017 tentang Cekungan Airtanah di Indonesia. Jakarta. Kementerian Energi dan Sumber Daya Mineral*). (*In Indonesian*) https://jdih.esdm.go.id/index.php/web/result/1612/detail

Lee, K.-S., Wenner, D. B. and Lee, I. (1999): Using H-and O-isotopic data for estimating the relative contributions of rainy and dry season precipitation to groundwater: example from Cheju Island, Korea. Journal of Hydrology, 222, 1–4, 65–74. https://doi.org/10.1016/S0022-1694(99)00099-2

Liu, F., Song, X., Yang, L., Zhang, Y., Han, D., Ma, Y. and Bu, H. (2015): Identifying the origin and geochemical evolution of groundwater using hydrochemistry and stable isotopes in the Subei Lake basin, Ordos energy base, northwestern China. Hydrology & Earth System Sciences, 19, 1. https://doi.org/10.5194/hess-19-551-2015

Logeshkumaran, A., Magesh, N. S., Godson, P. S. and Chandrasekar, N. (2015): Hydro-geochemistry and application of water quality index (WQI) for groundwater quality assessment, Anna Nagar, part of Chennai City, Tamil Nadu, India. Applied Water Science, 5, 4, 335–343. https://doi.org/10.1007/s13201-014-0196-4

Lubis, R. F., Sakura, Y. and Delinom, R. (2008): Groundwater recharge and discharge processes in the Jakarta groundwater basin, Indonesia. Hydrogeology Journal, 16, 5, 927–938. https://doi.org/10.1007/s10040-008-0278-1

Marandi, A. and Shand, P. (2018): Groundwater chemistry and the Gibbs Diagram. Applied Geochemistry, 97, 209–212. https://doi.org/10.1016/j.apgeochem.2018.07.009

Marsal, D. (1987): Statistics for geoscientists (translated from German by D. F. MERRIAM) (1st Ed.). Pergamon Press.

Mirčovski, V., Gičevski, B. and Dimov, G., (2018): Hydrochemical characteristics of the groundwaters in Prilep's part of Pelagonia valley – Republic of Macedonia. *Rudarsko-geološko-Naftni Zbornik*, 33, 3, 111-119. Retrieved from https://hrcak.srce.hr/ojs/index.php/rgn/article/view/6496

Mulyadi. (1985): The Geophysical Investigation of Banten Geothermal Area, West Java. 7th NZ Geothermal Workshop, 201–206. https://www.geothermal-energy.org/pdf/IGAstandard/NZGW/1985/Mulyadi.pdf

Oyuntsetseg, D., Ganchimeg, D., Minjigmaa, A., Ueda, A. and Kusakabe, M. (2015): Isotopic and chemical studies of hot and cold springs in western part of Khangai Mountain region, Mongolia, for geothermal exploration. Geothermics, 53, 488–497. https://doi.org/10.1016/j.geothermics.2014.08.010

Pentecost, A., Jones, B. and Renaut, R. W. (2003): What is a hot spring? Canadian Journal of Earth Sciences, 40, 11, 1443–1446. https://doi.org/10.1139/e03-083

Piper, A. M. (1944): A graphic procedure in the geochemical interpretation of water-analyses. Eos, Transactions American Geophysical Union, 25, 6, 914–928. https://doi.org/10.1029/TR025i006p00914

Rusydi, A. F. (2018): Correlation between conductivity and total dissolved solid in various type of water: A review. IOP Conference Series: Earth and Environmental Science, 118, 1, 12019. IOP Publishing. https://doi.org/10.1088/1755-1315/118/1/012019

Srinivasamoorthy, K., Gopinath, M., Chidambaram, S., Vasanthavigar, M. and Sarma, V. S. (2014): Hydrochemical characterization and quality appraisal of groundwater from Pungar sub basin, Tamilnadu, India. Journal of King Saud University-Science, 26, 1, 37–52. https://doi.org/https://doi.org/10.1016/j.jksus.2013.08.001

Suryadarma and Fauzi, A. (1991): Hydrothermal Alteration of The Garung Banten Geothermal Area West Java. Proc.13th New Zealand Geothermal Workshop, 193–197. Retrieved from https://www.geothermal-energy.org/pdf/IGAstandard/NZGW/1991/Suryadarma.pdf

Suryaman, M. (1999): Hydrogeological Map of Indonesia, Scale 1:100.000, Directorate of Environmental Geology, Bandung. Indonesia. (unpublished reports)

Tabachnick, B. G. and Fidell, L. S. (2013): Using multivariate statistics (6th ed.): Pearson Boston, MA, 983p.

Taniguchi, M., Nakayama, T., Tase, N. and Shimada, J. (2000): Stable isotope studies of precipitation and river water in the Lake Biwa basin, Japan. Hydrological Processes, 14, 3,

539–556. https://doi.org/10.1002/(SICI)1099-1085(20000228)14:3%3C539::AID-HYP953%3E3.0.CO;2-L

Tizro, A. T. and Voudouris, K. S. (2008): Groundwater quality in the semi-arid region of the Chahardouly basin, West Iran. Hydrological Processes: An International Journal, 22, 16, 3066–3078. https://doi.org/10.1002/hyp.6893

Tóth, J. (1999): Groundwater as a geologic agent: an overview of the causes, processes, and manifestations. Hydrogeology Journal, 7(1), 1–14. https://doi.org/10.1007/s100400050176

Tweed, S., Leblanc, M., Cartwright, I., Bass, A., Travi, Y., Marc, V., Bach, T.N., Duc, N.D., Massuel1, S and Kumar, U. S. (2019): Stable Isotopes of Water in Hydrogeology. Encyclopedia of Water: Science, Technology, and Society, edited by Patricia A. Maurice. https://doi.org/10.1002/9781119300762.wsts0154

Villegas, P., Paredes, V., Betancur, T., Taupin, J. D. and Toro, L. E. (2018): Groundwater evolution and mean water age inferred from hydrochemical and isotopic tracers in a tropical confined aquifer. Hydrological Processes, 32, 14, 2158–2175. https://doi.org/10.1002/hyp.13160

Zhang, Y., Xu, M., Li, X., Qi, J., Zhang, Q., Guo, J., Yu, L. and Zhao, R. (2018): Hydrochemical characteristics and multivariate statistical analysis of natural water system: A case study in Kangding County, Southwestern China. Water, 10, 1, 80. https://doi.org/10.3390/w10010080

Zhang, Yuqi., Zhou, X., Liu, H., Yu, M., Hai, K., Tan, M. and Huo, D. (2019): Hydrogeochemistry, geothermometry, and genesis of the hot springs in the Simao Basin in southwestern China. Geofluids, 2019. https://doi.org/10.1155/2019/7046320

SAŽETAK

Podrijetlo i kvaliteta podzemnih voda bazena Rawadanau, Serang Banten, Indonezija

Rawadanau je područje tropske, planinske močvare u Serangu (Banten), Indonezija. Tamošnje podzemne vode glavni su izvor opskrbe industrijskoga područja Cilegon, Banten. Poznavanje njihova podrijetla i kvalitete može pomoći u očuvanju toga resursa. Cilj je ovoga rada objasniti podrijetlo tih voda s novim podatcima o stabilnim izotopima (^{18}O i ^2H) te hidrokemijskim podatcima. Terenska mjerenja uključila su pH, temperaturu, EC, HCO_3^-, a analiza kationa, aniona i stabilnih izotopa napravljena je u laboratoriju. Postojeći izvori vode uključuju izvore, bušotine i rijeke. Načinjena je hijerarhijska analiza klastera na temelju kemije vode i stabilnih izotopa. Izdvojena su dva klastera: K (K1 i K2) te L. Podatci $\delta^{18}O$ i δ^2H iz izvora upućuju na meteorsko podrijetlo vode te na evaporaciju iz nekoliko njih. Meteorska voda sa sadržajem stabilnih izotopa $\delta^{18}O$ između –6,39 i –4,82 ‰ te δ^2H od –41,35 do –31,30 ‰ određena je dvama procesima, tj. otapanjem stijena i evaporacijom. Vodonosnici su sastavljeni od vulkanskih stijena pretežito od porfiritskoga i bazaltnoga andezita te andezita. Multivarijantna statistička analiza svih varijabli (osim pH i SO_4^{2-}), tj. većine kationa i aniona, pokazala je znatnu korelaciju. Izdvojena su 4 hidrokemijska facijesa podzemne vode, redom: $Ca-HCO_3$, $Ca-Mg-HCO3$, $Mg-Ca-HCO_3$ i $Na-Cl$.

Ključne riječi:
Rawadanau; podzemna voda; podrijetlo; stabilni izotopi; hidrokemijski facijesi; izvor

Author's contribution

Priyo Hartanto (1) (PhD student, senior researcher, hydrogeology) was in charge of manuscript writing, sampling and measurements and data analysis and gave possible conclusions of this research. **Boy Yoseph CSS Syah Alam (2)** (Dr., associate professor, hydrochemical) was in charge of hydrochemical analysis data. **Rachmat Fajar Lubis (3)** (Dr., senior researcher, hydrogeology) was in charge of manuscript writing and took part in the sampling, measurements and data analysis. **Hendarmawan Hendarmawan (4)** (Full Professor, hydrogeology) was in charge of the isotope analysis and overall manuscript structure as well. All authors were the main contributors.